

Binarization-Aware Adjuster: Bridging Continuous Optimization and Binary Inference in Edge Detection

Hao Shu*

* Sun-Yat-Sen University, Shenzhen, China.

* Shenzhen University, Shenzhen, China.

Abstract—Image edge detection (ED) faces a fundamental mismatch between training and inference: models are trained using continuous-valued outputs but evaluated using binary predictions. This misalignment, caused by the non-differentiability of binarization, weakens the link between learning objectives and actual task performance. In this paper, we propose a theoretical method to design a Binarization-Aware Adjuster (BAA), which explicitly incorporates binarization behavior into gradient-based optimization. At the core of BAA is a novel loss adjustment mechanism based on a Distance Weight Function (DWF), which reweights pixel-wise contributions according to their correctness and proximity to the decision boundary. This emphasizes decision-critical regions while down-weighting less influential ones. We also introduce a self-adaptive procedure to estimate the optimal binarization threshold for BAA, further aligning training dynamics with inference behavior. Extensive experiments across various architectures and datasets demonstrate the effectiveness of our approach. Beyond ED, BAA offers a generalizable strategy for bridging the gap between continuous optimization and discrete evaluation in structured prediction tasks.

I. INTRODUCTION

Image edge detection (ED) is a fundamental task in computer vision, serving as a critical component for higher-level applications such as segmentation, inpainting, and object recognition [1–3]. While ED has advanced significantly—from early classical methods [4, 5] to modern deep learning-based approaches [6–10], a core theoretical inconsistency remains underexplored.

This inconsistency lies in the gap between the continuous-valued outputs used for training and the binary predictions required at inference. Ground-truth edge maps are binary, indicating the presence or absence of edges at each pixel. However, to enable gradient-based optimization, models are trained to produce continuous values in $[0, 1]$, typically using loss functions such as binary cross-entropy (BCE). Because binarization is discontinuity, it is excluded from the training loop and applied only post hoc during evaluation. This disconnect can lead to suboptimal performance: a model that minimizes the training loss may not yield the most accurate binary predictions after thresholding.

In practice, a fixed threshold is used to convert predicted probabilities into a binary edge map. Predictions near this

threshold are inherently uncertain and more prone to misclassification, making them especially critical to the final binary outcome. In contrast, confidently correct predictions, namely those far from the threshold and on the correct side, have limited impact on the binary result, but they often dominate the loss due to their ease of optimization. As a result, standard continuous-value loss functions allocate excessive learning capacity to uninformative regions while neglecting the more decision-critical predictions near the decision threshold. This imbalance impairs the effectiveness of training and may ultimately degrade binary performance.

While prior work has improved ED performance through architectural innovations [6, 7, 10] and alternative loss functions [11–13], few have addressed the theoretical misalignment between continuous-valued training objectives and binary evaluation metrics. The binarization step remains disconnected from the optimization process, leaving a fundamental gap in the learning framework.

To address this, we propose a theoretical method to design a binarization-aware adjuster (BAA) that explicitly incorporates binarization behavior into the training process. Central to our method is a novel threshold-aware loss adjustment mechanism that dynamically modulates each pixel’s contribution to the loss based on its proximity to the decision threshold and correctness. Predictions near the threshold or those misclassified receive higher weights, while confidently correct predictions are down-weighted. This principled adjustment redirects the learning signal toward decision-critical regions, aligning optimization objectives with the binary nature of the task.

Our main contributions are as follows:

- We identify a core mismatch in ED: the disconnect between continuous-valued supervision in model training and binary-valued final output in practical usage, and propose the BAA method to resolve it.
- We introduce a principled method for constructing BAA based on Distance Weight Function (DWF), and demonstrate how it generalizes and improves upon loss formulations.
- We validate our approach through extensive experiments across multiple benchmark datasets and architectures, demonstrating the effectiveness of the proposed method.

II. PREVIOUS WORKS

This section reviews the landscape of ED research across datasets, model architectures, loss functions, and evaluation protocols, with an emphasis on foundational developments and persisting challenges.

A. Datasets

Early ED research relied heavily on datasets designed for related tasks such as contour detection and image segmentation. Notable benchmarks like BSDS300 and BSDS500 [14], featuring multi-annotator contour labels, remain widely used. Other commonly adopted datasets include MDBD [15] for boundary detection, NYUD [16] for semantic segmentation, and general-purpose datasets such as PASCAL VOC [17], COCO [18], SceneParse150 [19], and Cityscapes [20]. However, these were not originally designed for ED.

As the field matured, specialized ED datasets emerged. BIPED and its improved version BIPED2 [21] introduced high-resolution single-edge annotations. BRIND [6] extended the annotations of BSDS500 with semantically labeled edges, including reflectance, illumination, normal, and depth. UDED [22] offered fewer samples but prioritized annotation quality and consistency, enabling more reliable evaluation.

Nevertheless, annotation quality remains a key bottleneck. Human-labeled edge maps often suffer from noise, inconsistency, and semantic ambiguity. Although several studies have proposed more robust training strategies and refined labeling protocols [23–25], annotation noise continues to challenge both model generalization and fair benchmarking.

B. Model Architectures

The evolution of ED models can be divided into three phases: classical heuristics, early learning-based methods, and deep learning-driven approaches.

Classical methods such as the Sobel operator [4] and Canny detector [5] used hand-crafted gradient filters to capture intensity discontinuities. While computationally efficient, these methods lack adaptability to semantic structures and struggle in complex visual environments.

Early learning-based models incorporated statistical learning using manually crafted features like texture descriptors [26], sketch tokens [27], or histogram-based cues [28], paired with classifiers such as structured forests [29] or logistic regression [30]. However, these approaches were fundamentally limited by their reliance on hand-engineered features and had limited generalization across diverse scenes.

The advent of deep learning, particularly convolutional neural networks (CNNs), opened a new path for ED. HED [11] introduced deep supervision across network layers from multiple resolutions, while RCF [31] and BDCN [32] refined the multi-scale fusion techniques. Models such as PiDiNet [33] and DexiNet [34] focused on designing new structures for improving ED prediction. Beyond CNNs, transformer-based methods [7, 35] and diffusion-based approaches [8, 9] explore global context modeling and have also been employed in ED-related tasks, though their advantages in the ED task itself

remain under study. Recently, the Extractor-Selector (E-S) paradigm [10] introduced a two-stage framework combining feature extraction with a learnable selection module, offering a new perspective on the challenge of discriminative feature selection.

C. Loss Functions

Loss function design plays a critical role in ED. The Weighted Binary Cross-Entropy (WBCE) loss remains the most widely adopted approach, emphasizing edge pixels to address the low recall rate of the BCE loss. Despite its effectiveness in obtaining a high recall rate, WBCE often requires non-maximum suppression (NMS) at inference time to obtain clean, thin edge maps, resulting in a trade-off between quantitative score and prediction quality.

To address this, various alternative loss functions have been proposed. Dice loss [36] emphasizes region-level overlap, while tracing loss [37] targets the proportion of edges within edge-adjacent areas. Ranking-based approaches, such as RankED [12] and AP-loss [38], aim to enhance precision by optimizing pixel-level ranking. More recently, SWBCE [13] accounts for human uncertainty by rebalancing the contributions of edge and non-edge regions.

While these advanced losses provide perceptual or structural improvements, they often introduce new challenges such as instability, reduced precision, or sensitivity to hyperparameters, hindering their widespread use. A unified loss that aligns training supervision with binary evaluation, while maintaining stability and generalization, remains an open problem.

D. Evaluation Metrics

Standard evaluation metrics for ED were established by [26] and remain widely adopted. The two most common metrics are:

- **ODS (Optimal Dataset Score):** Best F_1 -score computed using a single optimal binarization threshold applied across the entire dataset.
- **OIS (Optimal Image Score):** Mean of best F_1 -scores computed per image using image-specific optimal thresholds.

These metrics are computed using an error-tolerance matching strategy to allow minor spatial misalignments. However, the error-tolerance radius is often dataset-specific and can influence results and comparability. Early works did not unify the error-tolerance benchmark among datasets until recent studies advocated for a fixed 1-pixel tolerance to ensure stricter, more consistent evaluation [25].

III. METHODOLOGY

A. Motivation and Insight

A key challenge in training ED models is the mismatch between training objectives and evaluation protocols. During training, ED models generate continuous-valued outputs in the range $[0, 1]$, typically optimized using pixel-wise loss functions such as WBCE. In contrast, evaluation metrics are computed on binarized edge maps, obtained by applying a

fixed threshold to these outputs. Since the binarization operation is discontinuous, it cannot be directly incorporated into the training process. This disconnect creates a fundamental issue: the loss function does not explicitly align with the discrete classification decisions that ultimately determine evaluation performance.

This gap introduces a critical inefficiency in optimization. Pixels whose predicted values lie on the correct side and far from the decision threshold, namely those correct pixels with high confidence, tend to dominate the gradient signal since they are easy to optimize. In contrast, pixels with predictions near the threshold, which are more ambiguous and critical to classification, contribute less to the gradients since they are more difficult to optimize. Consequently, the optimizer, driven by gradient magnitude, inadvertently prioritizes ‘easy’ but less effective pixels over ‘ambiguous’ but crucial ones, due to the nature of the optimization that tends to optimize the less-challenging pixels with higher priority. This misallocation of optimization effort can prevent the optimal parameter to be learned, resulting in suboptimal learning and degraded final performance.

For example, Table I reports optimal binarization thresholds for various ED models on multiple datasets under WBCE loss, which typically fall between 0.6 and 0.8. Suppose the binarization threshold is 0.7, then reducing the predicted value of a non-edge pixel from 0.50 to 0.01 has no effect on the final binary edge map, but it significantly reduces the loss. Moreover, such confident correct predictions are often easy to optimize. Indeed, it is because they are easy to optimize that they become the correctly predicted ones with high confidence. Therefore, training naturally prioritizes them for their optimization ease, even though further improvement on them yields no benefit for the final decision. In contrast, increasing the predicted value of an edge pixel from 0.69 to 0.71 can be more difficult, which is the reason why its prediction is near the decision threshold. Therefore, though critical for correct classification, it contributes less to the loss and thus is more easily overlooked.

TABLE I
Optimal binarization thresholds under WBCE training: Evaluation uses 1-pixel error tolerance without NMS. Experimental settings follow the ones in Section IV-A. Models are retrained on the pre-training set and evaluated on the validation set.

	UDED	BSDS500	BRIND	BIPED2
HED	0.74	0.85	0.77	0.79
BDCN	0.65	0.79	0.78	0.72
Dexi	0.63	0.87	0.79	0.79
EES3-Double	0.61	0.86	0.77	0.80

To bridge the continuous optimization and the binarization inference, we propose a novel loss adjustment mechanism, realized by a BAA, that dynamically re-weights pixel-wise loss contributions based on both proximity to the decision threshold and classification correctness. By explicitly incorporating binarization behavior into the training process, The BAA method ensures that the model allocates its learning capacity to the most decision-critical pixels.

B. Adjusted Loss Function Formulation

Although designing the BAA is non-trivial, the idea of using an adjuster is conceptually simple. Let us first address the simpler task, formally defining the adjusted loss function in this subsection, and leave the more challenging part, designing the BAA, to the next.

We define an adjusted loss as a loss that incorporates a pixel-wise weighting factor:

$$L_{Adj,\delta}(Pred, Gt) = \sum_i (Adj(P_i, G_i) + \delta)L(P_i, G_i) \quad (1)$$

where i runs over all pixels, L is a selected baseline pixel-wise loss function such as WBCE¹, $Pred$ and Gt represent the model prediction and the ground truth, respectively, P_i and G_i represent the model prediction and the ground truth of the i -th pixel, respectively, and $\delta \geq 0$ is a pre-defined hyperparameter, directly adding loss L with intensity δ to the adjusted loss to stabilize training. The function Adj is called an **Adjuster**, where $Adj(P_i, G_i) \in [0, 1]$ assigns dynamic weights, emphasizing the training signal according to the pixel’s contribution to the final binary decision.

Despite the simple idea, the problem lies in the design of the adjuster. A naive choice of $Adj(P_i, G_i)$ is the binary mask $\hat{Adj}_{thr}(P_i, G_i)$, defined as:

$$\hat{Adj}_{thr}(P_i, G_i) = \begin{cases} 0 & \text{If } (P_i - thr)(G_i - thr) \geq 0 \\ 1 & \text{Otherwise} \end{cases} \quad (2)$$

where thr is the binarization threshold. Hence, $L_{Adj,\delta}$ satisfying (providing $\delta = 0$):

- If a pixel is correctly classified, then the loss on it is 0.
- If a pixel is incorrectly classified, then the loss on it is positive.

This adjuster emphasizes only misclassified pixels. However, the discontinuity of its corresponding adjusted loss function renders it unsuitable for gradient-based optimization. Therefore, a smoother, differentiable formulation is necessary.

C. Design of the Binarization-Aware Adjuster

Let thr denote the binarization threshold. The adjuster Adj we aim to construct should satisfy:

- *C1 (Continuity)*: The adjuster Adj must be continuous to allow gradient-based optimization.
- *C2 (Non – negativity)*, $Adj(P_i, G_i)$ should be non-negative since it represents the weight of a pixel. Without loss generality, assume that $Adj(P_i, G_i) \in [0, 1]$, since multiplying a constant provides no essential difference.
- *C3 (Uncertainty Emphasis)*: If a pixel is correctly classified, then the closer the prediction is to thr , the higher the weight $Adj(P_i, G_i)$ of it should be, reflecting the loss caused by the uncertainty.
- *C4 (Confidence Saturation)*: If a pixel is correctly classified with high confidence (i.e., prediction far from thr), then $Adj(P_i, G_i)$ should decay to 0 quickly as P_i goes away from thr , representing that further optimizing

¹The same symbol L is employed to denote both the loss function on a single pixel ($L(P_i, G_i)$) and on the whole image ($L(Pred, Gt)$).

provide little benefits. Indeed, $Adj(P_i, G_i)$ should close to the maximal value when P_i close to thr , remain large when P_i is not far from thr , and decay to 0 after some pre-defined distance thr_dev .

- *C5 (Classification Sensitivity)*: If a pixel is misclassified, namely if it is an edge one but $P_i < thr$ or is a non-edge one but $P_i \geq thr$, its weight $Adj(P_i, G_i)$ should be maximal, representing correctly classification is of the first priority.

These conditions ensure that misclassified pixels always receive full attention, and optimization of correct pixels is focused on the uncertain parts while conserving effort on highly confident correct parts. We call an adjuster satisfying the above conditions a **Binarization-Aware Adjuster**, abbreviated as **BAA** for short. Namely:

Definition 1: A Binarization-Aware Adjuster (BAA) regarding $thr \in [0, 1]$ and $thr_dev > 0$ is a function $[0, 1]^2 \rightarrow [0, 1]$ satisfying the above conditions C1 to C5.

Let thr_dev denote the threshold window from C4. To construct a BAA, we define that:

Definition 2: A function $f_{thr_dev}(x)$ is said to be a Distance Weight Function (DWF) regarding the threshold window $thr_dev \in \mathbb{R}_+$, if it satisfies the following properties:

- *Continuity*: $f_{thr_dev}(x) : [0, thr_dev] \rightarrow [0, 1]$ is continuous.
- *Monotonically Decreasing*: $f_{thr_dev}(x_1) \leq f_{thr_dev}(x_2)$, $\forall x_1, x_2 \in [0, thr_dev]$ with $x_1 \geq x_2$. (or equivalently, $\frac{df_{thr_dev}}{dx}(x) \leq 0$ for differentiable $f_{thr_dev}(x)$).
- *Concavity*: $f(\lambda x_1 + (1-\lambda)x_2) \geq \lambda f(x_1) + (1-\lambda)f(x_2)$, $\forall x_1, x_2 \in [0, thr_dev]$ and $\lambda \in [0, 1]$. (or equivalently, $\frac{d^2 f_{thr_dev}}{dx^2}(x) \leq 0$ for secondary differentiable $f_{thr_dev}(x)$).
- *Boundary Conditions*: $f_{thr_dev}(0) = 1$, and $f_{thr_dev}(thr_dev) = 0$.

Then:

$$\widetilde{Adj}(P_i, G_i) = \begin{cases} f_{thr_dev}(|P_i - thr|) & 0 \leq |P_i - thr| \leq thr_dev \\ 0 & |P_i - thr| > thr_dev \end{cases} \quad (3)$$

satisfies C1 – C4.

An example of the DWF $f_{thr_dev}(x) = f_{b,thr_dev}(x)$ can be constructed as:

$$f_{b,thr_dev}(x) = \frac{e^{b \times x} - e^{b \times thr_dev}}{1 - e^{b \times thr_dev}} \quad (4)$$

i.e.,

$$\lim_{b \rightarrow +\infty} BAA_{thr,b,thr_dev}(P_i, G_i) = \widetilde{Adj}_{thr,thr_dev}(P_i, G_i) \quad (11)$$

This confirms that the BAA bridges the binarization logic with the continuous-loss gradient-based training. Furthermore, let also $thr_dev \rightarrow 0^+$, then it is reduced to \hat{Adj}_{thr} from Equation 2.

where $b \geq 0$ is pre-defined, controlling the decay rate.

To also meet C5, we define the masked distance as:

Definition 3: The $([0, 1])$ masked distance $MD_{thr}(x, y) : [0, 1]^2 \rightarrow [0, 1]$ regarding the threshold $thr \in [0, 1]$ is defined as:

$$MD_{thr}(x, y) = (x - thr) \times y + (thr - x) \times (1 - y) \quad (5)$$

Hence, $MD_{thr}(P_i, G_i)$ measures both the correctness and confidence of the pixel i . For a wrongly predicted pixel i , namely whose prediction is on the different side of the thr as its ground truth value, $MD_{thr}(P_i, G_i) \leq 0$, while for a correctly predicted pixel i , $MD_{thr}(P_i, G_i)$ is the L^1 distance of P_i from the binarization threshold thr .

Now, a BAA can be defined as:

$$BAA_{thr,thr_dev}(P_i, G_i) = \hat{f}_{thr_dev}(MD_{thr}(P_i, G_i)) \quad (6)$$

where \hat{f}_{thr_dev} is an extension of a selected DWF $f_{thr_dev}(x)$, defined as:

$$\hat{f}_{thr_dev}(x) = \begin{cases} 1 & x < 0 \\ f_{thr_dev}(x) & 0 \leq x \leq thr_dev \\ 0 & x > thr_dev \end{cases} \quad (7)$$

D. Theoretical Properties of the BAA

To better understand the proposed adjuster's behavior, we analyze its mathematical properties. Let $f_{thr_dev}(x) = f_{b,thr_dev}(x)$ be defined as in Equations 4 and $\hat{f}_{thr_dev}(x) = \hat{f}_{b,thr_dev}(x)$ be its extension defined in Equation 7. Then $\hat{f}_{b,thr_dev}(x)$ serves as a smooth approximation to a hard binarization function. Specifically, it generalizes the discrete threshold-based binary weighting function $B_{thr_dev}(x)$ on threshold thr_dev , defined as:

$$B_{thr_dev}(x) = \begin{cases} 1 & x < thr_dev \\ 0 & x \geq thr_dev \end{cases} \quad (8)$$

The two functions coincide as $b \rightarrow +\infty$:

$$\lim_{b \rightarrow +\infty} \hat{f}_{b,thr_dev}(x) = B_{thr_dev}(x) \quad (9)$$

Therefore, the extended function \hat{f}_{b,thr_dev} is a continuous approximation for threshold logic $B_{thr_dev}(x)$. Accordingly, the map $BAA_{thr,thr_dev}(P_i, G_i) = BAA_{thr,b,thr_dev}(P_i, G_i)$, defined by Equation 6, converges to a discrete decision-based adjuster $\widetilde{Adj}_{thr,thr_dev}(P_i, G_i)$, defined as follow:

$$\widetilde{Adj}_{thr,thr_dev}(P_i, G_i) = \begin{cases} 0 & (P_i - thr)(G_i - thr) \geq 0 \ \& \ |P_i - thr| \geq thr_dev \\ 1 & \text{Otherwise} \end{cases} \quad (10)$$

Moreover, for a DWF $f_{thr_dev}(x)$, the following bounds holds:

$$1 - \frac{x}{thr_dev} \leq f_{thr_dev}(x) \leq 1 \quad (12)$$

Therefore:

$$\lim_{thr_dev \rightarrow +\infty} f_{thr_dev}(x) = 1 \quad (13)$$

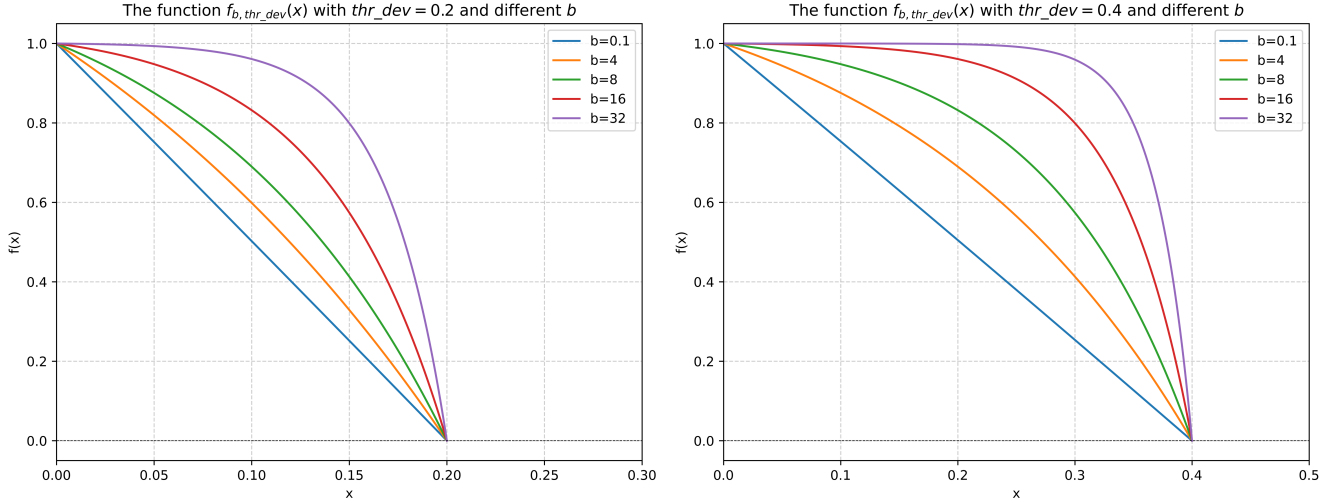


Fig. 1 The different choices of b in the DWF $f_{b,thr_dev}(x)$ presented in Equation 4

which implies that:

$$\lim_{thr_dev \rightarrow +\infty} BAA_{thr,thr_dev}(x) = 1 \quad (14)$$

and the adjusted loss $L_{Adj,\delta}$ defined in Equation 1 degenerates to the baseline loss L up to a constant:

$$\lim_{thr_dev \rightarrow \infty} L_{Adj,\delta}(Pred, Gt) = (1 + \delta)L(Pred, Gt) \quad (15)$$

In summary, the proposed adjusted loss function $L_{Adj,\delta}$ with $Adj = BAA_{thr,b,thr_dev}$ defined above by the DWF in Equation 4, generalizes the baseline loss L . It degenerates to the baseline loss when $thr_dev \rightarrow +\infty$, converges to a binary weighted loss when $b \rightarrow +\infty$, and maintains the continuity². These asymptotic behaviors confirm that the constructed BAA bridges the continuous loss and post-binarization classification, aligning training with downstream evaluation in ED.

E. Hyperparameter Selection and Training Protocol

The proposed BAA depends on three hyperparameters: thr : binarization threshold, thr_dev : threshold window beyond which correct predictions are ignored in optimization, and b (when employing $f_{b,thr_dev}(x)$ from Equation 4 as the DWF): DWF decay rate,

The DWF decay rate b occurs specifically in the DWF defined in Equation 4, controlling the concavity of $f_{b,thr_dev}(x)$, determining how sharply the adjusted weight decays as predictions diverge from the decision boundary thr . Its effect is illustrated in Figure 1, and we set $b = 16$ as the default.

thr_dev defines the margin around thr within which a correct prediction is considered uncertain. A correct prediction with $|P_i - thr| > thr_dev$ is considered as confidently correct and receives zero weight. We empirically choose $thr_dev = 0.2$.

thr is the most critical hyperparameter in the BAA. Experiments (Table I) show that the optimal value for ED models typically lies between 0.6 and 0.8, so we use $thr = 0.7$ as the default.

²Here, $\delta = 0$ is provided.

However, given its importance, it is worth providing a calibration method for it. Specifically, we suggest a self-adaptive thr chosen by pre-training: pre-train the model on a sub-dataset without applying BAA and evaluate the pre-trained model on a validation set to select a suitable thr for BAA.

Therefore, the final training protocol of an ED model M under a selected baseline loss function L on a dataset D , with the presented BAA method can be formulated as:

- Step 1: Split D into pre-train set PT , validation set V , and test set T .
- Step 2: Train M on PT using baseline loss L , and evaluate on V to estimate thr .
- Step 3: Retrain M via $L_{BAA,\delta}$, on $PT \cup V$, and evaluate finally on T .

In experiments, δ is simply set to be 1.

IV. EXPERIMENT

This section presents experiments designed to evaluate the proposed method.

A. Experimental Setting

To assess the effectiveness of the proposed binarization adjustment mechanism, we adopt the adjuster designed by Equation 4, 5, 6, and 7 as the BAA, and WBCE as the baseline loss function L , due to its widespread use in ED tasks.

1) *Baseline and Benchmark*: The proposed method is evaluated across a range of ED models, including:

- HED (2015) [11].
- BDCN (2022) [32].
- Dexi (2023) [34].
- EES3-Double (2025) [10], the EES framework, integrating the above three models with the double-size selector.

Experiments are conducted on four benchmark datasets:

- BRIND [6].
- BSDS500 [14].
- UDED [22].
- BIPED2 [21].

All models are retrained from scratch on each dataset to ensure fairness. For consistency and simplicity, only the final output of each model is used for supervision, bypassing any need for hyperparameter tuning in intermediate layers. Each model is trained under the following three configurations of loss function for comparison:

- Standard WBCE (baseline).
- WBCE with a fixed-threshold BAA using $thr = 0.7$ (denoted as *BAA-0.7*).
- WBCE with a self-adaptive adjuster where thr is automatically selected following the method in Section III-E (denoted as *BAA-SA*).

Unless otherwise specified, the hyperparameters for the adjusted loss defined by the BAA are fixed at $thr_{dev} = 0.2$, $b = 16$, and $\delta = 1$.

Evaluation protocols follow the standard ED metrics (ODS and OIS) introduced in [26], under the strictest 1-pixel error tolerance without post-processing techniques such as non-maximal-suppression (NMS), suggested in [25]. The evaluations under the traditional relaxed error tolerance (4.3 to 11.1 pixels) with NMS are provided in the appendix.

2) *Dataset Partitions and Augmentation*: Dataset preprocessing and postprocessing procedures follow those introduced in [10]. Details are stated as follows.

The dataset partitions are:

- BRIND and BSDS500: 400 training images, 100 testing images.
- UDED: 20 training images, 7 testing images (excluding two images with resolution below 320×320).
- BIPED2: 200 training images, 50 testing images.

For training under the self-adaptive adjuster setting in section III-E, each training set is further divided into pre-training and validation subsets:

- BRIND and BSDS500: 300 pre-training, 100 validation images.
- UDED: 15 pre-training, 5 validation images.
- BIPED2: 150 pre-training, 50 validation images.

Data augmentations are applied, including:

- Halving the images until both height and width are strictly below 640 pixels.
- Rotations at four angles, 0° , 90° , 180° , and 270° , with horizontal flips.
- Addition of noiseless data.

3) *Training Note*: During training, input images are randomly cropped to 320×320 and refreshed every 5 epochs. The batch size is set to 8. All models are trained on an A100 GPU using Adam optimizer, with a learning rate of 0.0001 and a weight decay of 10^{-8} .

Training runs for 200 epochs on UDED and 50 epochs on the remaining datasets.

4) *Inference Method*: In the inference phase, each image is split into overlapping 320×320 patches with a stride of 304 pixels (i.e., 16 pixels overlap). The model predicts edge maps on each patch independently, and the outputs are aggregated to form the final edge map.

Further implementation details can be found in the codes or in [10].

B. Experimental Result

Tables II and III report the ED performance of all methods on BRIND, BSDS500, UDED, and BIPED2 datasets under the strict 1-pixel error tolerance setting, without applying NMS. The evaluation includes ODS and OIS scores for each configuration.

TABLE II

Results on BRIND and BSDS500 under 1-pixel error tolerance without NMS: For BRIND, all annotations per image are merged into a single binary ground truth map, where a pixel is considered an edge one if it is marked as such by any annotator. For BSDS500, only label 1 is used as the ground truth. Notations follow those introduced in the main-text. The best scores for each model are highlighted in **bold**. Rows labeled *A*, *A-BAA-0.7*, and *A-BAA-SA* represent the average performance across the four models, while *Improvement* rows indicate the relative improvements over the baseline.

	BRIND		BSDS500	
	ODS	OIS	ODS	OIS
HED (2015)	0.664	0.673	0.444	0.455
HED-BAA-0.7	0.668	0.676	0.441	0.453
HED-BAA-SA	0.664	0.672	0.455	0.465
BDCN (2022)	0.655	0.663	0.432	0.446
BDCN-BAA-0.7	0.662	0.671	0.445	0.452
BDCN-BAA-SA	0.665	0.674	0.454	0.468
Dexi (2023)	0.675	0.683	0.465	0.473
Dexi-BAA-0.7	0.674	0.683	0.475	0.485
Dexi-BAA-SA	0.679	0.687	0.470	0.480
EES3-Double (2025)	0.683	0.690	0.488	0.504
EES3-Double-BAA-0.7	0.690	0.697	0.493	0.509
EES3-Double-BAA-SA	0.690	0.697	0.497	0.507
A	0.669	0.677	0.457	0.470
A-BAA-0.7	0.674	0.682	0.464	0.475
A-BAA-0.7-Improvement	+0.75%	+0.74%	+1.53%	+1.06%
A-BAA-SA	0.675	0.683	0.469	0.480
A-BAA-SA-Improvement	+0.90%	+0.89%	+2.63%	+2.13%

TABLE III

Results on UDED and BIPED2 under 1-pixel error tolerance without NMS: Notations follow the ones in TableII.

	UDED		BIPED2	
	ODS	OIS	ODS	OIS
HED (2015)	0.709	0.742	0.630	0.633
HED-BAA-0.7	0.727	0.755	0.629	0.634
HED-BAA-SA	0.712	0.748	0.633	0.635
BDCN (2022)	0.688	0.723	0.636	0.639
BDCN-BAA-0.7	0.713	0.741	0.637	0.639
BDCN-BAA-SA	0.712	0.749	0.640	0.643
Dexi (2023)	0.700	0.738	0.643	0.648
Dexi-BAA-0.7	0.721	0.752	0.640	0.646
Dexi-BAA-SA	0.731	0.765	0.641	0.646
EES3-Double (2025)	0.751	0.780	0.670	0.673
EES3-Double-BAA-0.7	0.762	0.794	0.671	0.675
EES3-Double-BAA-SA	0.758	0.791	0.675	0.680
A	0.712	0.746	0.645	0.648
A-BAA-0.7	0.731	0.761	0.644	0.649
A-BAA-0.7-Improvement	+2.67%	+2.01%	-0.16%	+0.15%
A-BAA-SA	0.729	0.763	0.647	0.651
A-BAA-SA-Improvement	+2.39%	+2.28%	+0.31%	+0.46%

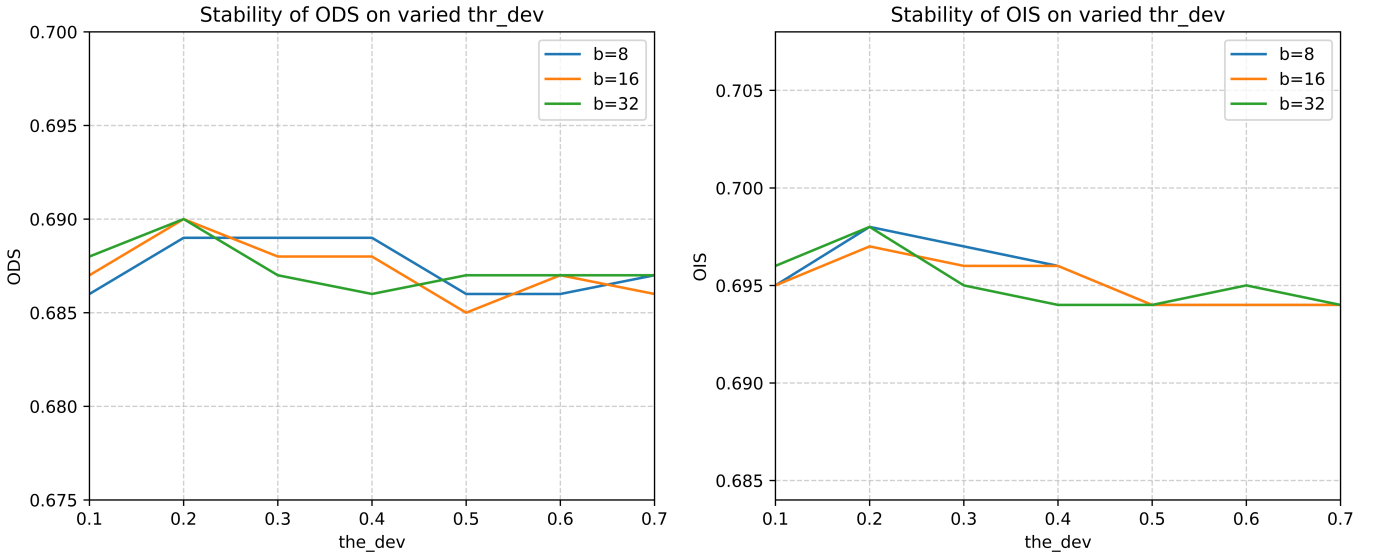


Fig. 2 ODS and OIS across thr_dev : Figures show how ODS and OIS vary with thr_dev values from 0.1 to 0.7, across different decay rates b (8, 16, 32). Experiments are conducted on BRIND using the EES3-Double model and adjusted WBCE loss. Threshold thr is fixed at 0.7 and δ at 1.

The results clearly demonstrate that incorporating the proposed BAA method, whether with the fixed threshold (*BAA-0.7*) or the self-adaptive strategy (*BAA-SA*), leads to improvements in performance across most models and datasets.

Both variants of the BAA loss improve the baseline WBCE loss across all models and datasets. The self-adaptive version (*BAA-SA*) tends to achieve slightly better performance than the fixed threshold in most cases.

On BRIND, the best ODS gains are observed in BDCN (about +1.5%) using the self-adaptive adjuster (*BAA-SA*). On BSDS500, EES3-Double and BDCN benefit most from the adjuster, with ODS improvements up to +1.8% and +2.6%, respectively. UDED shows the most significant performance gains. The average ODS improves by about +2.7% (*BAA-0.7*) and +2.4% (*BAA-SA*) compared to the baseline. On BIPED2, the improvements are modest but consistent with *BAA-SA* outperforming both baseline and fixed-threshold setups.

These results strongly validate the effectiveness of the proposed BAA method, especially the self-adaptive variant. The method is robust across different backbone architectures and datasets, offering consistent improvements with minimal modifications to the existing training pipeline.

C. Ablation Study

Figure 2 illustrates how ODS and OIS scores vary with different values of thr_dev (from 0.1 to 0.7) and decay rates b (8, 16, 32) in the DWF (Equation 4). All experiments are conducted on the BRIND dataset using the EES3-Double model trained with the BAA-WBCE loss. The threshold thr is fixed at 0.7, and δ at 1.

This ablation study shows that across all tested configurations, $thr_dev = 0.2$ consistently yields the best performance. Also, the proposed BAA method is robust to a wide range of hyperparameter settings, which simplifies hyperparameter tuning and reinforces the general applicability of the method.

V. CONCLUSION

This paper tackles a fundamental yet underexplored issue in image edge detection (ED): the misalignment between the continuous-valued outputs optimized during training and the binary predictions required at inference and evaluation. This discrepancy, often overlooked due to the discontinuity of binarization, undermines the alignment between training objectives and final task performance.

To address this, we propose a principled binarization adjustment mechanism that incorporates binarization awareness into the training process. Guided by the Distance Weight Function (DWF), the Binarization-Aware Adjuster (BAA) adaptively modulates each pixel’s contribution to the loss based on its prediction correctness and confidence. It downweights confidently correct predictions since further optimizing them has little effect on the binary output, while emphasizing ambiguous or misclassified regions that are more critical to the final binarization decision. The resulting adjusted loss function from the BAA generalizes traditional loss formulations and embeds binarization behavior directly into the optimization process. In addition, we introduce a self-adaptive training procedure to dynamically estimate an appropriate binarization threshold for the BAA, further aligning training dynamics with inference behavior.

Extensive experiments across diverse models and datasets validate the effectiveness and robustness of the proposed method. Beyond ED, our BAA approach can also provide a theoretical method for bridging the gap between continuous optimization and discrete evaluation, offering a promising direction for broader applications in structured prediction tasks such as segmentation and classification.

REFERENCES

- [1] K. Nazeri, E. Ng, T. Joseph, F. Qureshi, and M. Ebrahimi. Edgeconnect: Structure guided image inpainting using edge prediction. In *2019 IEEE/CVF International Conference on Computer Vision Workshop (ICCVW)*, pages 3265–3274, 2019.
- [2] R. Muthukrishnan and M. Radha. Edge detection techniques for image segmentation. *International Journal of Computer Science & Information Technology*, 3(6):259, 2011.
- [3] C. H. Zhan, X. H. Duan, S. Y. Xu, Z. Song, and M. Luo. An improved moving object detection algorithm based on frame difference and edge detection. In *Fourth international conference on image and graphics (ICIG 2007)*, pages 519–523. IEEE, 2007.
- [4] J. Kittler. On the accuracy of the sobel edge detector. *Image and Vision Computing*, 1(1):37–42, 1983.
- [5] J. Canny. A computational approach to edge detection. *IEEE Transactions on pattern analysis and machine intelligence*, PAMI-8(6):679–698, 1986.
- [6] M. Pu, Y. Huang, Q. Guan, and H. Ling. Rindnet: Edge detection for discontinuity in reflectance, illumination, normal and depth. In *2021 IEEE/CVF International Conference on Computer Vision (ICCV)*, pages 6859–6868. IEEE Computer Society, oct 2021.
- [7] M. Y. Pu, Y. P. Huang, Y. M. Liu, Q. J. Guan, and H. B. Ling. Edter: Edge detection with transformer. In *Proceedings of the IEEE/CVF conference on computer vision and pattern recognition*, pages 1402–1412, 2022.
- [8] C. x. Zhou, Y. P. Huang, M. C. Xiang, J. H. Ren, H. B. Ling, and J. Zhang. Generative edge detection with stable diffusion. *arXiv preprint arXiv:2410.03080*, 2024.
- [9] Y. F. Ye, K. Xu, Y. H. Huang, R. J. Yi, and Z. P. Cai. Diffusionedge: Diffusion probabilistic model for crisp edge detection. In *Proceedings of the AAAI conference on artificial intelligence*, volume 38, pages 6675–6683, 2024.
- [10] Hao Shu. Boosting edge detection with pixel-wise feature selection: The extractor-selector paradigm, 2025.
- [11] S. N. Xie and Z. W. Tu. Holistically-nested edge detection. In *Proceedings of the IEEE international conference on computer vision*, pages 1395–1403, 2015.
- [12] B. Cetinkaya, S. Kalkan, and E. Akbas. Ranked: Addressing imbalance and uncertainty in edge detection using ranking-based losses. In *Proceedings of the IEEE/CVF Conference on Computer Vision and Pattern Recognition*, pages 3239–3249, 2024.
- [13] Hao Shu. Rethinking edge detection through perceptual asymmetry: The swbce loss, 2025.
- [14] D. Martin, C. Fowlkes, D. Tal, and J. Malik. A database of human segmented natural images and its application to evaluating segmentation algorithms and measuring ecological statistics. In *Proc. 8th Int'l Conf. Computer Vision*, volume 2, pages 416–423, July 2001.
- [15] D. A. Mély, J. k. Kim, M. McGill, Y. L. Guo, and T. Serre. A systematic comparison between visual cues for boundary detection. *Vision Research*, 120:93–107, 2016. Vision and the Statistics of the Natural Environment.
- [16] N. N. Silberman, D. Hoiem, P. P. Kohli, and R. Fergus. Indoor segmentation and support inference from rgb-d images. In *European Conference on Computer Vision*, 2012.
- [17] M. Everingham, L. Van Gool, C. K. I. Williams, J. Winn, and A. Zisserman. The pascal visual object classes (voc) challenge. *International Journal of Computer Vision*, 88(2):303–338, jun 2010.
- [18] T. Y. Lin, M. Maire, S. Belongie, L. Bourdev, R. Girshick, J. Hays, P. Perona, D. Ramanan, C. L. Zitnick, and P. Dollár. Microsoft coco: Common objects in context. In *Computer Vision – ECCV 2014*, pages 740–755. Springer International Publishing, 2014.
- [19] B. L. Zhou, H. Zhao, X. Puig, S. Fidler, A. Barriuso, and A. Torralba. Scene parsing through ade20k dataset. In *2017 IEEE Conference on Computer Vision and Pattern Recognition (CVPR)*, pages 5122–5130, 2017.
- [20] M. Cordts, M. Omran, S. Ramos, T. Rehfeld, M. Enzweiler, R. Benenson, U. Franke, S. Roth, and B. Schiele. The cityscapes dataset for semantic urban scene understanding. In *Proceedings of the IEEE Conference on Computer Vision and Pattern Recognition (CVPR)*, June 2016.
- [21] X. Soria, E. Riba, and A. Sappa. Dense extreme inception network: Towards a robust cnn model for edge detection. In *2020 IEEE Winter Conference on Applications of Computer Vision (WACV)*, pages 1912–1921. IEEE Computer Society, mar 2020.
- [22] X. Soria, Y. Li, M. Rouhani, and A. D. Sappa. Tiny and efficient model for the edge detection generalization. In *2023 IEEE/CVF International Conference on Computer Vision Workshops (ICCVW)*, pages 1356–1365. IEEE Computer Society, oct 2023.
- [23] Y. B. Fu and X. J. Guo. Practical edge detection via robust collaborative learning. In *Proceedings of the 31st ACM International Conference on Multimedia, MM '23*, page 2526–2534. Association for Computing Machinery, 2023.
- [24] C. Wang, D. Dai, S. Xia, Y. Liu, and G. Wang. One-stage deep edge detection based on dense-scale feature fusion and pixel-level imbalance learning. *IEEE Transactions on Artificial Intelligence*, 5(01):70–79, jan 2024.
- [25] Hao Shu. Enhancing edge detection by texture handling architecture and noiseless training data. 2025.
- [26] D.R. Martin, C.C. Fowlkes, and J. Malik. Learning to detect natural image boundaries using local brightness, color, and texture cues. *IEEE Transactions on Pattern Analysis and Machine Intelligence*, 26(5):530–549, 2004.
- [27] J. J. Lim, C. L. Zitnick, and P. Dollár. Sketch tokens: A learned mid-level representation for contour and object detection. In *Proceedings of the IEEE conference on computer vision and pattern recognition*, pages 3158–3165, 2013.
- [28] P. Arbeláez, M. Maire, C. Fowlkes, and J. Malik. Contour detection and hierarchical image segmentation. *IEEE Transactions on Pattern Analysis and Machine Intelli-*

- gence, 33(5):898–916, 2011.
- [29] P. Dollár and C. L. Zitnick. Fast edge detection using structured forests. *IEEE Transactions on Pattern Analysis and Machine Intelligence*, 37(8):1558–1570, 2015.
- [30] X. F. Ren. Multi-scale improves boundary detection in natural images. In *Computer Vision–ECCV 2008: 10th European Conference on Computer Vision, Marseille, France, October 12-18, 2008, Proceedings, Part III 10*, pages 533–545. Springer, 2008.
- [31] Y. Liu, M. M. Cheng, X. W. Hu, K. Wang, and X. Bai. Richer convolutional features for edge detection. In *Proceedings of the IEEE conference on computer vision and pattern recognition*, pages 3000–3009, 2017.
- [32] J. Z. He, S. L. Zhang, M. Yang, Y. H. Shan, and T. J. Huang. Bdcn: Bi-directional cascade network for perceptual edge detection. *IEEE Transactions on Pattern Analysis and Machine Intelligence*, 44(1):100–113, 2022.
- [33] Z. Su, W. Z. Liu, Z. T. Yu, D. W. Hu, Q. Liao, Q. Tian, M. Pietikäinen, and L. Liu. Pixel difference networks for efficient edge detection. In *Proceedings of the IEEE/CVF international conference on computer vision*, pages 5117–5127, 2021.
- [34] X. Soria, A. Sappa, P. Humanante, and A. Akbarinia. Dense extreme inception network for edge detection. *Pattern Recognition*, 139:109461, 2023.
- [35] J. H. Jie, Y. Guo, G. X. Wu, J. M. Wu, and B. J. Hua. Edgenat: Transformer for efficient edge detection. *arXiv preprint arXiv:2408.10527*, 2024.
- [36] R. X. Deng, C. H. Shen, S. J. Liu, H. B. Wang, and X. R. Liu. Learning to predict crisp boundaries. In *Computer Vision – ECCV 2018: 15th European Conference, Munich, Germany, September 8–14, 2018, Proceedings, Part VI*, page 570–586. Springer-Verlag, 2018.
- [37] L. X. Huan, N. Xue, X. W. Zheng, W. He, J. Y. Gong, and G. S. Xia. Unmixing convolutional features for crisp edge detection. *IEEE Trans. Pattern Anal. Mach. Intell.*, 44(10 Part 1):6602–6609, oct 2022.
- [38] K. Chen, J. G. Li, W. Y. Lin, J. See, J. Wang, L. Y. Duan, Z. B. Chen, C. W. He, and J. N. Zou. Towards accurate one-stage object detection with ap-loss. In *Proceedings of the IEEE/CVF Conference on Computer Vision and Pattern Recognition*, pages 5119–5127, 2019.

VI. APPENDIX

A. Evaluation on Relaxed Benchmark

Tables IV and V present the evaluation results under the traditional relaxed criterion, with the pixel error tolerance ranging from 4.3 to 11.1 pixels, depending on the resolution of the evaluated image, and using NMS.

TABLE IV
Results on BRIND and BSDS500 with 4.3-pixel error tolerance and NMS: Notations follow those used in the main-text.

	BRIND		BSDS500	
	ODS	OIS	ODS	OIS
HED (2015)	0.781	0.795	0.613	0.630
HED-BAA-0.7	0.786	0.798	0.618	0.639
HED-BAA-SA	0.781	0.793	0.629	0.642
BDCN (2022)	0.770	0.783	0.609	0.631
BDCN-BAA-0.7	0.778	0.791	0.618	0.634
BDCN-BAA-SA	0.779	0.791	0.622	0.645
Dexi (2023)	0.788	0.800	0.642	0.663
Dexi-BAA-0.7	0.791	0.804	0.648	0.673
Dexi-BAA-SA	0.791	0.803	0.639	0.651
EES3-Double (2025)	0.792	0.804	0.651	0.680
EES3-Double-BAA-0.7	0.797	0.809	0.649	0.670
EES3-Double-BAA-SA	0.797	0.808	0.654	0.663
A	0.683	0.796	0.629	0.651
A-BAA-0.7	0.688	0.801	0.633	0.654
A-BAA-0.7-Improvement	+0.73%	+0.63%	+0.64%	+0.46%
A-BAA-SA	0.687	0.799	0.636	0.650
A-BAA-SA-Improvement	+0.59%	+0.38%	+1.11%	-0.15%

TABLE V
Results on UDED and BIPED2 with 0.0075 error tolerance and NMS: Notations follow those used in the main-text. A 0.0075 error tolerance corresponds to approximately 11.1-pixel tolerance for BIPED2.

	UDED		BIPED2	
	ODS	OIS	ODS	OIS
HED (2015)	0.806	0.846	0.883	0.890
HED-BAA-0.7	0.818	0.849	0.884	0.892
HED-BAA-SA	0.807	0.843	0.883	0.890
BDCN (2022)	0.786	0.822	0.883	0.890
BDCN-BAA-0.7	0.798	0.828	0.881	0.889
BDCN-BAA-SA	0.801	0.832	0.886	0.893
Dexi (2023)	0.788	0.824	0.887	0.895
Dexi-BAA-0.7	0.801	0.831	0.884	0.892
Dexi-BAA-SA	0.814	0.858	0.886	0.894
EES3-Double (2025)	0.831	0.858	0.888	0.896
EES3-Double-BAA-0.7	0.834	0.863	0.889	0.897
EES3-Double-BAA-SA	0.832	0.859	0.890	0.898
A	0.803	0.838	0.885	0.893
A-BAA-0.7	0.813	0.843	0.885	0.894
A-BAA-0.7-Improvement	+1.25%	+0.60%	+0.00%	+0.11%
A-BAA-SA	0.814	0.848	0.886	0.894
A-BAA-SA-Improvement	+1.37%	+1.19%	+0.11%	+0.11%

B. Full Data Used in Ablation Study

Table VI provides the detailed numerical data used to generate Figure 2 in the ablation study.

TABLE VI

Hyperparameter Evaluation for thr_dev and b : Results are reported on the BRIND dataset under 1-pixel error tolerance without NMS, corresponding to Figure 2. The table lists ODS and OIS scores for various combinations of thr_dev and b , while keeping $thr = 0.7$ and $\delta = 1$. Notations follow those in the main-text.

BRIND with 1-pixel error tolerance without NMS		
Hyperparameter: thr - thr_dev - δ - b	ODS	OIS
EES3-Double-Adj: 0.7-0.1-1-8	0.686	0.695
EES3-Double-Adj: 0.7-0.2-1-8	0.689	0.698
EES3-Double-Adj: 0.7-0.3-1-8	0.689	0.697
EES3-Double-Adj: 0.7-0.4-1-8	0.689	0.696
EES3-Double-Adj: 0.7-0.5-1-8	0.686	0.694
EES3-Double-Adj: 0.7-0.6-1-8	0.686	0.694
EES3-Double-Adj: 0.7-0.7-1-8	0.687	0.694
EES3-Double-Adj: 0.7-0.1-1-16	0.687	0.695
EES3-Double-Adj: 0.7-0.2-1-16	0.690	0.697
EES3-Double-Adj: 0.7-0.3-1-16	0.688	0.696
EES3-Double-Adj: 0.7-0.4-1-16	0.688	0.696
EES3-Double-Adj: 0.7-0.5-1-16	0.685	0.694
EES3-Double-Adj: 0.7-0.6-1-16	0.687	0.694
EES3-Double-Adj: 0.7-0.7-1-16	0.686	0.694
EES3-Double-Adj: 0.7-0.1-1-32	0.688	0.696
EES3-Double-Adj: 0.7-0.2-1-32	0.690	0.698
EES3-Double-Adj: 0.7-0.3-1-32	0.687	0.695
EES3-Double-Adj: 0.7-0.4-1-32	0.686	0.694
EES3-Double-Adj: 0.7-0.5-1-32	0.687	0.694
EES3-Double-Adj: 0.7-0.6-1-32	0.687	0.695
EES3-Double-Adj: 0.7-0.7-1-32	0.687	0.694